2021-02-19

# Statistical modeling of received signal strength for an FSO link over maritime environment

Lionis, Antonios; Peppas, Konstantinos; Nistazakis, Hector E.; Tsigopoulos, Andreas

Elsevier

Lionis, Antonios, et al. "Statistical modeling of received signal strength for an FSO link over maritime environment." Optics Communications 489 (2021): 126858. http://hdl.handle.net/10945/67379

Optics Communications 489 (2021) 126858

Contents lists available at ScienceDirect

Optics Communications

journal homepage: www.elsevier.com/locate/optcom

# Statistical modeling of received signal strength for an FSO link over maritime environment

Antonios Lionis [a], Konstantinos Peppas [a], Hector E. Nistazakis [b,*], Andreas Tsigopoulos [c], Keith Cohn [d]

[a] Information and Telecommunications Department, University of Peloponnese, Greece
[b] Section of Electronic Physics and Systems, Department of Physics, National and Kapodistrian University of Athens, Panepistimiopolis Zografou, Athens 15784, Greece
[c] Division of Combat Systems, Naval Operations, Sea Sciences, Navigation, Electronics & Telecommunications Sector, Hellenic Naval Academy, Greece
[d] Physics Department, Naval Postgraduate School, CA, USA

ARTICLE INFO

*Keywords:*
Free space optical communication
Received signal strength indicator
Atmospheric turbulence
Refractive index structure parameter
Navy Surface Layer Model

ABSTRACT

Free space optical communications (FSO) have the potential to substantially improve communications technology in terms of channel capacity and offer an alternative to their RF counterpart. Additional characteristics related to security, immunity, flexibility and low cost issues render FSO a reasonable candidate for military applications. FSO technology does not come without challenges. Its major issue is the local meteorological parameters that give rise to various atmospheric phenomena. The purpose of this work is to facilitate the performance prediction of an FSO communication link over a maritime environment by utilizing macroscopic meteorological parameters, i.e. air temperature, wind speed, relative humidity, air pressure, dew point, solar radiation and sea temperature, obtained from point measurements. The received signal strength indicator (RSSI) of the FSO receiver has been utilized as the performance metric of the channel and a closed form expression has been deduced. The model has then been validated against real meteorological data and the predicted RSSI values exhibited a reasonably strong correlation with the observed ones. Atmospheric turbulence has been taken into account using the Navy Surface Layer Model (NAVSLaM) to estimate the structure index parameter from the same meteorological data and thus allowed for a statistical correlation between the refractive index structure parameter and RSSI.

## 1. Introduction

The ever-increasing demands on reliable and high-speed data transfer lead the way to the current research efforts to advance the optical wireless communications (OWC) technology so it can be exploited by both small and light platforms. FSO systems offer significant advantages over RF technology due to their higher carrier frequency, the smaller size of their components, the more secure channel and the increased modulation bandwidth [1]. Therefore, platforms with size, weight and power constraints can benefit from more compact communication systems while achieving higher performance [2]. FSO technology applications span from fixed point to point networks, e.g. LAN, last mile access, fiber backup, to high speed moving platforms, e.g. UAVs, aircrafts, [3,4]. The applied laser technology level allows not only for terrestrial but also for underwater and space applications [5,6]. The major drawback that the FSO systems face is the various atmospheric phenomena that play a negative role on their performance. Weather effects such as haze, rain, snow, fog, etc, cause the scattering and absorption of the laser beam in a timescale of several minutes, whereas the atmospheric turbulence causes scintillation and beam wandering in a timescale of milliseconds [7]. These deleterious effects exhibit a rather different behavior in a maritime environment as compared to the terrestrial one [8,9]. Therefore, exhaustive research in such an environment is required in order to characterize the local weather effects on the FSO performance, [10].

Over the past few years, several research teams have established experimental setups in various terrains in order to acquire a better understanding of the atmospheric effects to the laser propagation and consequently to an FSO link. For example, the Chesapeake Bay Detachment of the Naval Research Laboratory has launched an extensive campaign towards the characterization of the atmosphere for a maritime laser link. A simple 100-m link over land was the first step to validate an optical turbulence model (PAMELA) through a twelve-month collection data period [11,12]. Following that, scintillation measurements for different aperture sizes have been conducted

* Corresponding author.
*E-mail addresses:* lionisantonios@gmail.com (A. Lionis), peppas@uop.gr (K. Peppas), enistaz@phys.uoa.gr (H.E. Nistazakis), atsigo@hna.gr (A. Tsigopoulos), krcohn@nps.edu (K. Cohn).

https://doi.org/10.1016/j.optcom.2021.126858
Received 26 October 2020; Accepted 6 February 2021
Available online 19 February 2021

over a 470-m maritime path [13]. Finally, an extended 16-km laser-comm link has been established over sea between Chesapeake Beach, MD and Tilghman Island, MD to characterize atmospheric turbulence, atmospheric transmission, angle-of-arrival fluctuations, bit error ratio and a variety of other atmospheric parameters [14]. Later on, an asymmetric link has been established by employing special retro-reflectors arrays to close a 32.4-km total maritime path [15–17]. In a rapid development effort, the Advanced Lasercom Systems and Operations group at MIT Lincoln Laboratory fielded two self-developed FSO terminals and established a 5.4-km terrestrial optical path. The collected data have been used to assess link performance as a function of system parameters with and without forward error correction [18,19]. Those field measurements also demonstrated the effectiveness of spatial diversity by reducing the fading-induced received optical power probability density function width. The influence of atmospheric environment on a terrestrial FSO link has been studied in [20–22] using statistical analysis of the optical received power and simple polynomial models were constructed to relate the RSSI with measured atmospheric parameters. Alheadary et al. explores solely the effects of temperature and humidity of a coastal environment on FSO communications [23,24]. In their work, two mathematical models are proposed to link the FSO attenuation coefficient with the air temperature, the humidity and the dew point. Tunick, studied the refractive index and the microclimate fluctuations effects to free-space laser communications by comparing scintillometer data with in-situ measurements of temperature variations [25] and calculated values of refractive index structure parameter ($C_n^2$) and Fried parameter ($r_0$) [26]. The probability density function, fade statistics and high frequency spectrum have been obtained based on experimental data that covered all seasons and collected from a 11.8-km urban terrain optical link in [27]. The performance of FSO transmission in terms of Packet Delivery Ratio (PDR) has been studied in a harsh weather environment in Qatar University along a 600-m long laser communication link [28]. Finally, the Hellenic Naval Academy has conducted extended applied research in maritime laser communications performance presented in [29–31].

The main goal of this study is to use a large data set obtained of a commercial FSO link with an over-water propagation path, located at the entrance of Piraeus port, during the winter of 2020, in order to gain a better understanding of the effects of atmospheric conditions to the performance of the link. Apparently, experimenting with a laser link in the open sea for extended period of time is not trivia; therefore, we utilized an established link between two fixed points on the land that crosses a maritime environment and allows for adequate experimental data to be obtained. A twenty two-day data collection period has been used to construct our proposed model for RSSI as a function of local environmental conditions, i.e. air temperature, wind speed, dew point, humidity, pressure, solar radiation and air–sea temperature difference, with a very decent approximation ($R^2 = 71\%$). The model has been validated and exhibited better accuracy as compared to our, elsewhere [31], proposed RSSI model. Finally, a $C_n^2$ parameter estimation model in maritime environment (NAVSLaM), proposed by the meteorology department of the Naval Postgraduate School, has been employed to correlate the measured RSSI parameter with the estimated atmospheric turbulence strength.

The remainder of this work is organized as follows. Section 2, provides the background of atmospheric turbulence and presents the NAVSLaM model for $C_n^2$ estimates in maritime environment. Section 3, describes the whole experimental setup, located across the entrance of Piraeus port. Section 4, presents and analyzes the findings of the measurements, whereas Section 5 concludes the paper.

## 2. Optical turbulence in the atmosphere

The atmosphere can be considered as a fluid with two distinct states of motion i.e. laminar and turbulent [32]. What distinguishes these two states is uniformity of velocity characteristics determined by a non-dimensional quantity called the Reynolds number [32]. According to the energy cascade theory of turbulence, when wind speed increases, this number overcomes the critical value and results in local unstable air masses, i.e. turbulent eddies [1]. These eddies are formed in different sizes, ranging from $L_0$ (outer range) down to $l_0$ (inner range). The outer range can have a diameter of up to 100-m and the inner up to 10-mm. Both are linearly correlated with height [32]. Assuming atmospheric fluctuations are homogeneous and isotropic, the structure function within outer and inner range, i.e the inertial subrange, follows a two-thirds power law, i.e. a $r^{2/3}$ dependence for a random variable *x(r)* is given as:

$$D_x\left(r_{(.)}\right) = D_x(f\left(\vec{r_1}, \vec{r_2}\right)) = \left\langle |x(\vec{r_1}) - x(\vec{r_2})|^2 \right\rangle \tag{1}$$

where $\vec{r_1}, \vec{r_2}$ the position vectors at two points separated by distance *r*. These atmospheric fluctuations can be associated with either parameter between wind velocity, temperature and refractive index. Turbulence fluctuations associated with the refractive index caused by temperature and pressure variations. The corresponding structure function for refractive index is given as:

$$D_n\left(r_n\right) = C_n^2 r^{2/3} \tag{2}$$

where $C_n^2$ stands for the refractive index structure parameter, a widely used term of turbulence strength characterization [31].

### 2.1. Forecasting optical turbulence

As described in the previous section, the effects of the weather conditions as well as other atmospheric phenomena have been extensively investigated both in a laboratory environment and in the field. The primary phenomenon that has been researched is the atmospheric turbulence since it is considered to have the most prominent degradation effects on a laser communications link. Several different experimental turbulence measurement methods exist, including predictive modeling of $C_n^2$ [33]. Usually, micrometeorology is required in order for one to be able to measure optical turbulence [34]. However, several models based upon local macro-meteorological parameters that can be easily obtained from a weather station, such as air temperature, wind speed, air pressure, etc., are available in the open technical literature. Representative examples are available in [34], which are mathematically expressed as simple regression models, with independent parameters that include wind speed, relative humidity, air temperature and solar flux. These models also include a weighting factor that favors the development of the bell-shaped diurnal profile of turbulence. Indeed, the models exhibit a correlation of 90% or more over a wide range of meteorological parameters values on a desert environment, [34]. However, upper and lower bounds of those values exist, that constrain the validity area of the models. Oermann in his work, [33], attempted to improve those models by adding the air-to-ground and air-to-air temperature differences as extra independent parameters. The developed model showed an improvement; however, since it utilized only daytime data it cannot be used for nighttime predictions. Recently, both models were utilized in [31] to correlate atmospheric turbulence strength with received signal strength over maritime environment and a moderate correlation was observed.

### 2.2. $C_n^2$ Predictive modeling for maritime environment

The focus of this paper is FSO performance assessment over a maritime environment, which exhibits significant differences with a terrestrial one.

A significant difference of a typical diurnal profile of atmospheric turbulence between a terrestrial and an over-water propagation path is that the latter does not exhibit reduced values around sunrise and sunset [35]. That means that the $C_n^2$ strength does not follow the characteristic bell-shaped diurnal profile but a random one during the day. Additionally, the $C_n^2$ strength over water is generally an order of magnitude lower than over land [7]. The FSO link availability as a

function of range was measured for specific set of FSO parameters for a desert, i.e. China Lake, CA, and a maritime i.e. Chesapeake Beach, MD, environments, and the former, as it would be expected, was much larger [7].

Over water, the atmospheric structure constant was found to have a strong dependence on the air–sea temperature difference (*ASTD*). Additionally, different beam propagation characteristics were observed for each temperature gradient sign. For colder air temperatures the beam transport is improved [35].

Apart from the expression of Eq. (2) for the refractive index structure parameter, valid for the inertial-subrange, $C_n^2$ can be expressed in terms of the temperature structure parameter, $C_T^2$, the specific humidity structure parameter, $C_q^2$, and the temperature-specific humidity cross-structure parameter, $C_{Tq}$, as:

$$C_n^2 = A^2 C_T^2 + 2ABC_{Tq} + B^2 C_q^2 \tag{3}$$

where $A$ and $B$ are the partial derivatives of refractive index with respect to temperature and specific humidity, respectively [36, Eqs. (16, 17)]. The Meteorology Department of the Naval Postgraduate School has developed a bulk $C_n^2$ prediction model based upon mean atmospheric layer properties, with an emphasis on the air–sea temperature difference. The model's basis is the Monin–Obukhov similarity (MOS) theory, which assumes conditions to be horizontally homogeneous and stationary and turbulent fluxes of momentum, sensible and latent heat, to be constant with height. These conditions are most likely to be valid in the open ocean rather than in a coastal location; therefore, the bulk model is believed to perform better in the former environment, [37]. Scaling parameters for wind speed, temperature and specific humidity are defined [37, Eq. (10)] as well as a universal parameter $\xi$ [37, Eq. (11)] which expresses any dynamic surface-layer property, made dimensionless by the scaling parameters. The mean vertical profiles of wind speed, temperature and specific humidity are also defined according to MOS theory [37, Eq. (12)]. Solving those profile expressions for the scaling parameters and combining the expressions of the structure parameters in terms of the scaling parameters with (2), results in the NAVSLaM model, [38],

$$C_n^2 = \frac{f(\xi)k^2[A^2\Delta T^2 + 2ABr_{Tq}\Delta T\Delta q + B^2\Delta q^2]}{z^{2/3}[\ln\left(\frac{z}{z_{oT}}\right) - \Psi_T(\xi)]^2} \tag{4}$$

and

$$\xi = \frac{zg(\Delta T + 0.61T\Delta q)[\ln\left(\frac{z}{z_{oU}}\right) - \Psi_U(\xi)]^2}{\theta_u \Delta U^2[\ln\left(\frac{z}{z_{oT}}\right) - \Psi_T(\xi)]} \tag{5}$$

where $f(\xi)$ is an empirical determined dimensionless function, $z$ the height above surface, $k$ the von Karman constant (≈0.4), $g$ the gravitational acceleration, $\theta_u$ the virtual potential temperature, $\Psi$ the integrated forms of the respective dimensionless profile functions, $z_{0T}$, $z_{0U}$, $z_{0q}$, i.e. the heights where the log-z profiles of $U$, $T$, $q$ reach their surface values and $r_{Tq}$ the temperature-specific humidity correlation coefficient.

By iteratively solving Eqs. (4) and (5), $C_n^2$ can be estimated after parameterizing $z_{oT}$ and $z_{oU}$ in terms of known quantity [37]. Full details on the NPS's NAVSLaM model are provided by Frederickson et al. [37]. After extended experimental analysis of the model, $C_n^2$ is found to have strong dependence on the absolute value of the air–sea temperature difference, increasing for higher wind speeds and negative *ASTD* and decreasing for positive *ASTD* values [37]. Compared to relative humidity, $C_n^2$ is directly proportional for positive *ASTD*, except for very small positive values [37]. The transition between positive and negative *ASTD* values was found to have a significant effect to the laser beam pointing [35]. Finally, its dependence on height was found to scale as $z^{-4/3}$ for unstable, i.e. $\xi < 0$, $z^{-2/3}$ for neutral, i.e. $\xi = 0$, and constant for stable, i.e. $\xi > 0$, conditions [37].

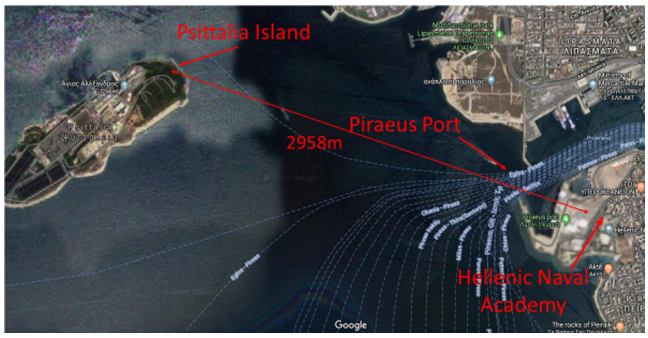


**Fig. 1.** The maritime optical communications link that connects the Hellenic Naval Academy and the lighthouse on Psittallia Island and has a total length of 2958 m.


**Fig. 2.** The MRV TS5000/155 FSO system on the roof of HNA's building. On its left is shown the Psittallia island where is located the second FSO system.

## 3. Measurement systems overview

An optical communications link has been established over a coastal maritime environment between the building of Hellenic Naval Academy and the lighthouse of Psitalia Island. The optical path length has an overall length of 2958 m, most of which is over sea, see Fig. 1. The link is assumed to be horizontal and seated at a height of 35 m over sea surface.

The FSO system used in the experiments is a commercial MRV TS500/155 transceiver, operating at 0.85 μm with a maximum output power of 150-mW and data rate of 155-Mbps. It utilizes three laser sources with a beam divergence of 2 mrad each and a single receiver with a diameter of 20-cm, sensitivity of −46-dBm and uses an avalanche photodetector (APD). It uses an open protocol to automatically identify and lock on the current data rate and clock (see Fig. 2).

The maritime optical link operates as a full-duplex link; however, the difficulty to access the Psitallia island site has led us to use this terminal as the transmitter and the HNA's terminal as the receiver. The received signal strength is measured, stored in a connected PC and exported to be analyzed. Collocated to the HNA's FSO system is a WS-2000 weather station which measures macroscopic environmental parameters, such as wind speed, air temperature, relative humidity, pressure, solar radiation and dew point.

## 4. Results and discussion

The experimental measurements took place during the winter of 2020. An initial period of twenty-two days, i.e. 24 January to 14 February, was devoted for data collection, analysis and model construction. Once per minute, the *RSSI* parameter was collected and logged

**Table 1**
The value range of the environmental parameters for the period 21 January to 14 February 2020.

| Parameter | Min value | Mean value | Max value |
|---|---|---|---|
| *RSSI* | 335.0 | 422.39 | 517.0 |
| *P* (hPa) | 987.7 | 1017.60 | 1035.3 |
| *T* (°C) | 273.8 | 282.80 | 290.7 |
| *RH*(%) | 41.0 | 69.61 | 93.0 |
| *DP* (°C) | −5.5 | 7.29 | 13.4 |
| *WS* (m/s) | 0.0 | 2.89 | 20.0 |
| *SF* (W/m$^2$) | 0.0 | 103.53 | 735.7 |
| *ASTD* (°C) | −11.1 | −2.23 | 5.7 |

from the MRV FSO system. That frequency was selected in order to easily correlate those measurements with the weather station's data collection, which include wind speed (*WS*), pressure (*P*), air temperature (*T*), dew point (*DP*), solar radiation (*SF*) and relative humidity (*RH*). Additionally, our model includes as an independent variable the air–sea temperature difference (*ASTD*). An online weather statistics database, [39], was exploited for the sea temperature measurements. The range of the environmental parameters values over this period is presented in Table 1.

As known, the relative humidity exhibits a significant anti-correlated behavior with temperature. This is the case between *ASTD* and *RH* too, as shown in Fig. 3.

On the other hand, the observed *RSSI* is shown a good agreement with the *ASTD* in terms of their fluctuation trends. The measurements "gap" during the 8-th of February is due to a temporary technical issue on the FSO system (see Fig. 4).

### 4.1. RSSI Statistical Modeling

The data collected during that period, i.e. 24 January to 14 February 2020, gave 26238 data points that allowed an accurate model construction to relate the *RSSI* with seven macroscopic environmental parameters. We used a linear regression analysis to construct a second-order model that would allow *RSSI* predictions based on environmental parameters point measurements. The regression analysis summary output showed a significant similarity between measured and predicted *RSSI* values, which are certified by an R-squared parameter value of 71.1%. A linear correlation coefficient was also used to numerically evaluate their analogy (0.843). The resulting regression model is given as,

$$\begin{aligned} RSSI = {} & 112100.8 + 21.4P - 0.01P^2 - 878.1T + 1.57T^2 \\ & + 10.47RH - 0.066RH^2 - 19.83DP + 0.52DP^2 - \\ & - 0.62WS - 0.09WS^2 + 0.12SF - 0.0001SF^2 \\ & - 7.8ASTD - 2.3ASTD^2 \end{aligned} \tag{6}$$

Fig. 5 presents a comparison between the *RSSI* values directly measured from the MRV FSO system, i.e. blue line and those predicted by our model, i.e. red line.

### 4.2. Model validation

In order to validate our model and its ability to predict the *RSSI* parameter from macroscopic environmental point-measurements, we selected two distinct periods, the first from 20 to 26 February 2020 and the second from 7 to 11 March 2020. The same environmental measurements were taken, and the observed RSSI value was compared with the predicted one. The environmental conditions during this period were pretty much the same with the collection data period. This fact is assumed to favor our model in terms of its predictability. As a comparison to the improved model, the *RSSI* parameter is also computed by our base model presented elsewhere [31]. It is observed that the inclusion of the *ASTD* as an independent parameter plays a key role to its improvement comparing to the base model. Fig. 6 shows the comparison between the observed, i.e. the blue line, base, i.e. red line and improved, i.e. yellow model. Our improved model achieves an $R^2$ parameter of 70.5%, which quantitatively supports its statistical significance. Qualitatively, it can be shown from Fig. 6 that the predicted parameters have a very good fit with the observed ones, even in harsh *RSSI* value differences as during the morning of the February 23th. Two minor failures are observed during the midday of the 24th and 25th of February where the model seems to underestimate the observed *RSSI* values. Overall, the improved model achieves a significant linear correlation coefficient of 0.78 with the observed values as compared to 0.73 of the base model.

The exact validation procedure is followed for the period from 7 to 11 of March 2020, where again our model proves its ability to make legitimate predictions for the *RSSI* parameter. Fig. 7 shows the comparison between the observed, base and improved models. Qualitatively, the improvement of the predictability of our model is apparent as compared to the base model which overestimated the *RSSI* parameter throughout the whole period, except two peak values observed during midday of 10th and 11th of March. The linear correlation coefficient comparison is slightly better for the improved model, i.e. 0.81 compared to 0.79. However this validity check has to do mainly with how good the model follows the general trend of the real measurements. As already stated, the base model has indeed an adequate correlation with the observed values, however it fails to accurately predict the real values. Finally, the improved model during this period exhibits less accuracy in terms of its $R^2$ parameter, i.e. 66%; however, it is still reliable for bulk estimations.

### 4.3. NAVSLaM $C_n^2$ predictions

A maritime environment exhibits different atmospheric phenomena and specialized models are required for atmospheric turbulence predictions in such an environment, as compared to predictions for a terrestrial one. This paper utilized such a model, i.e. NAVSLaM, to predict the $C_n^2$ strength along the propagation path of the link based on point measurements of macroscopic environmental parameters. Special attention is given to the effect of the air–sea temperature difference, since this parameter is found to have a significant impact to the turbulence behavior [35]. By solving Eqs. (4) and (5) in an iterative process, we estimated the $C_n^2$ during both validation periods and as a comparison we also estimated the $C_n^2$ utilizing other empirical models that are not focused on a maritime environment [34, Eqs. (12,13)]. A significant disagreement between model predictions is observed, a fact that justifies the different mechanisms of atmospheric turbulence over a maritime environment, so that maritime atmospheric turbulence cannot be predicted by a model focused on laser propagation over land. Figs. 8 and 9 show the turbulence fluctuation over two periods of times, i.e. 20 to 26 February and 7 to 11 March 2020.

The $C_n^2$ mean value for the first period is approximately $7.5\times10^{-16}$ $m^{-2/3}$, with a minimum of $3.5\times0^{-19}$ $m^{-2/3}$ and a maximum of $3.2\times10^{-15}$ $m^{-2/3}$. The equivalent values for the second period are, $2.2\times10^{-16}$ $m^{-2/3}$, $1.2\times10^{-18}$ $m^{-2/3}$ and $1.2\times10^{-15}$ $m^{-2/3}$. The values plotted in both figures are in logarithmic scale and a significant difference between the empirical models and NAVSLaM is apparent. Specifically, the prediction based on the empirical models has a mean value of approximately two orders of magnitudes higher and as known they exhibit a diurnal bell-shaped profile, with a maximum value around midday and minimum around the sunrise and sunset. This diurnal profile is not the case for turbulence over a maritime environment as shown in Figs. 8 and 9.

The $C_n^2$ predictions over both periods allowed an analysis of the effect of the turbulence strength to the received signal. Therefore, in Figs. 10 and 11 we plotted the *RSSI* parameter and the $C_n^2$ in logarithmic scale. In both periods, a strong anti-correlated relation was observed, demonstrating the deleterious effect of turbulence on the laser propagation.

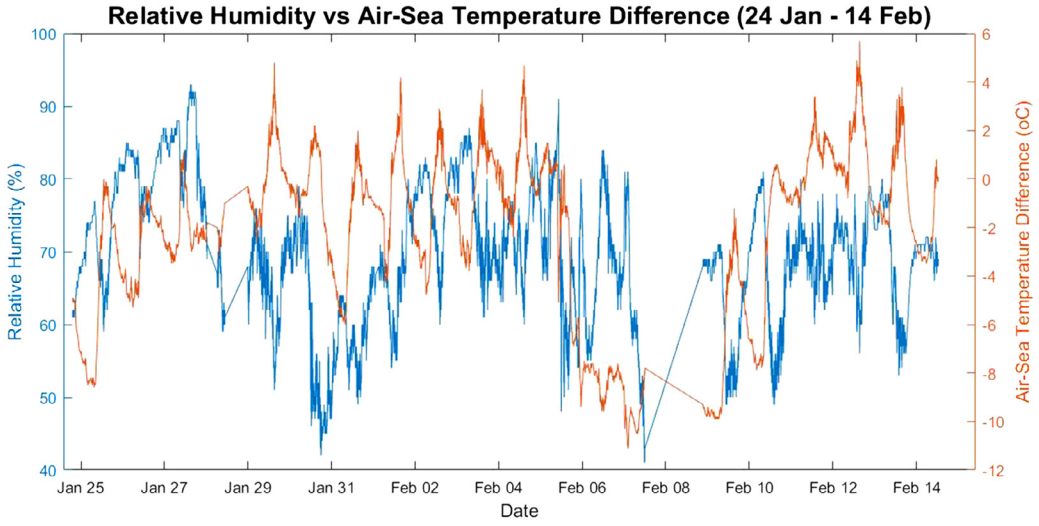


**Fig. 3.** The highly anti-correlated relation between relative humidity and air–sea temperature difference during the period 24 January to 14 February 2020.

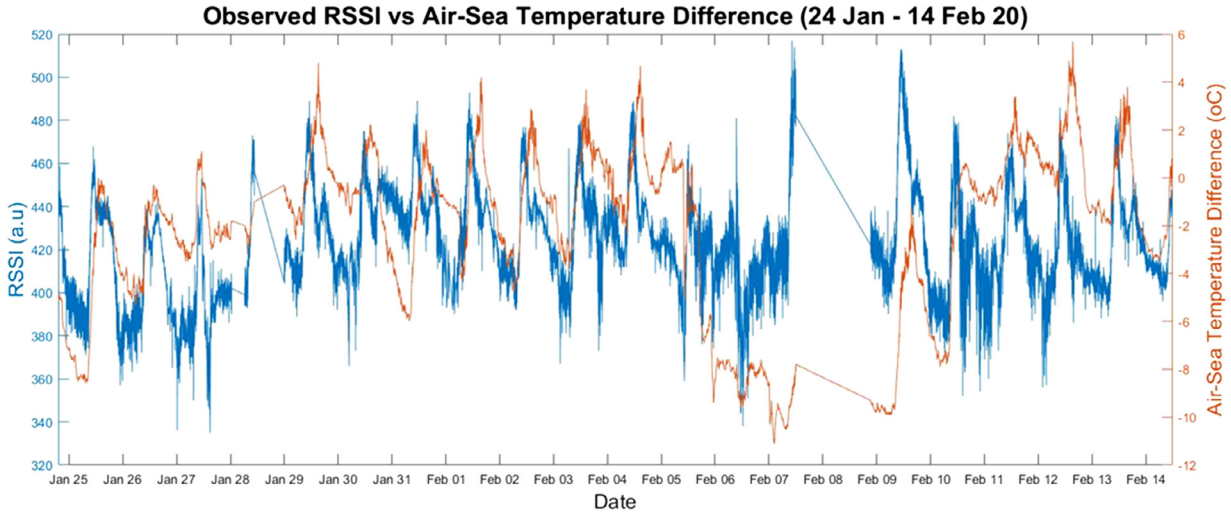


**Fig. 4.** Observed *RSSI* and air–sea temperature measurements comparison during the period 24 January to 14 February 2020.

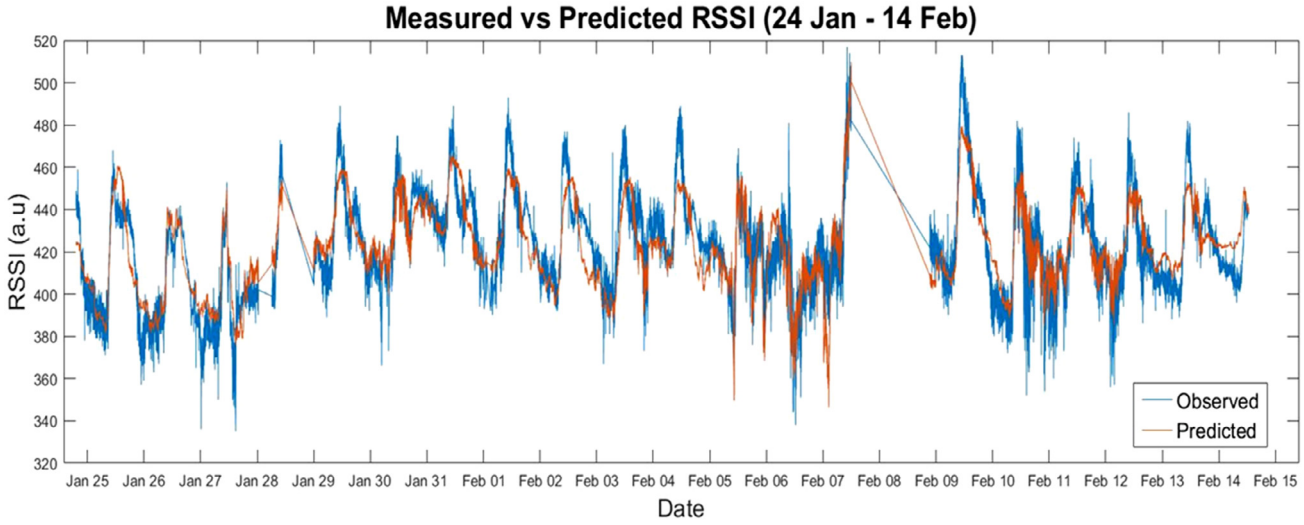


**Fig. 5.** Comparison between measured from FSO system and predicted from the model *RSSI* values for the period 24 January to 14 February 2020.

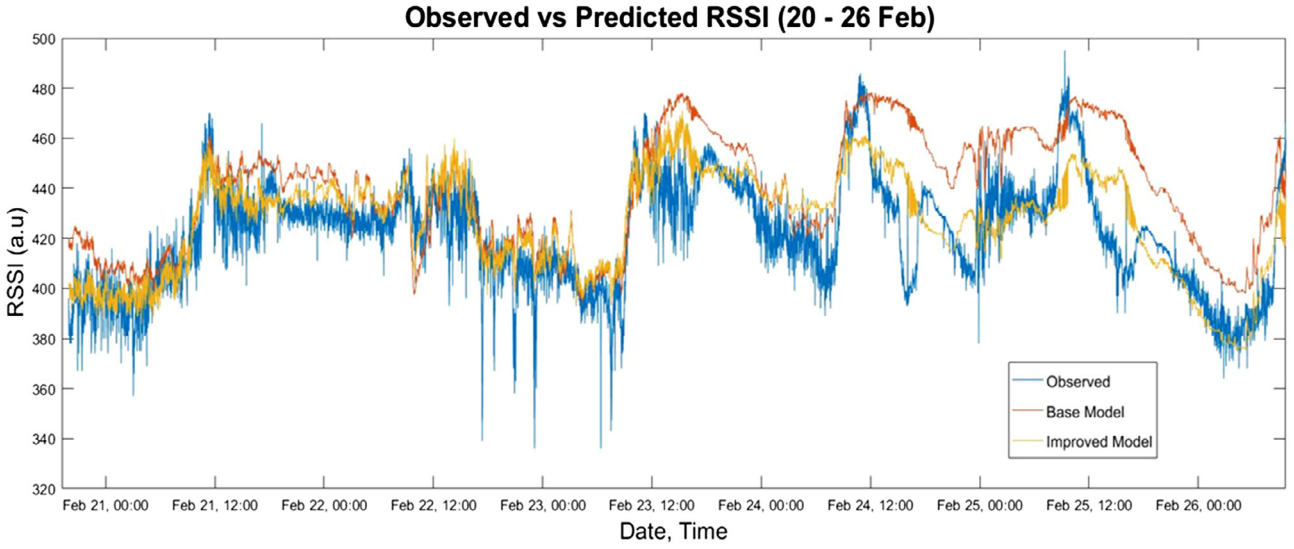


**Fig. 6.** Observed *RSSI* parameter as compared to both the base [32] and the improved model for the period from 20 to 26 February 2020.

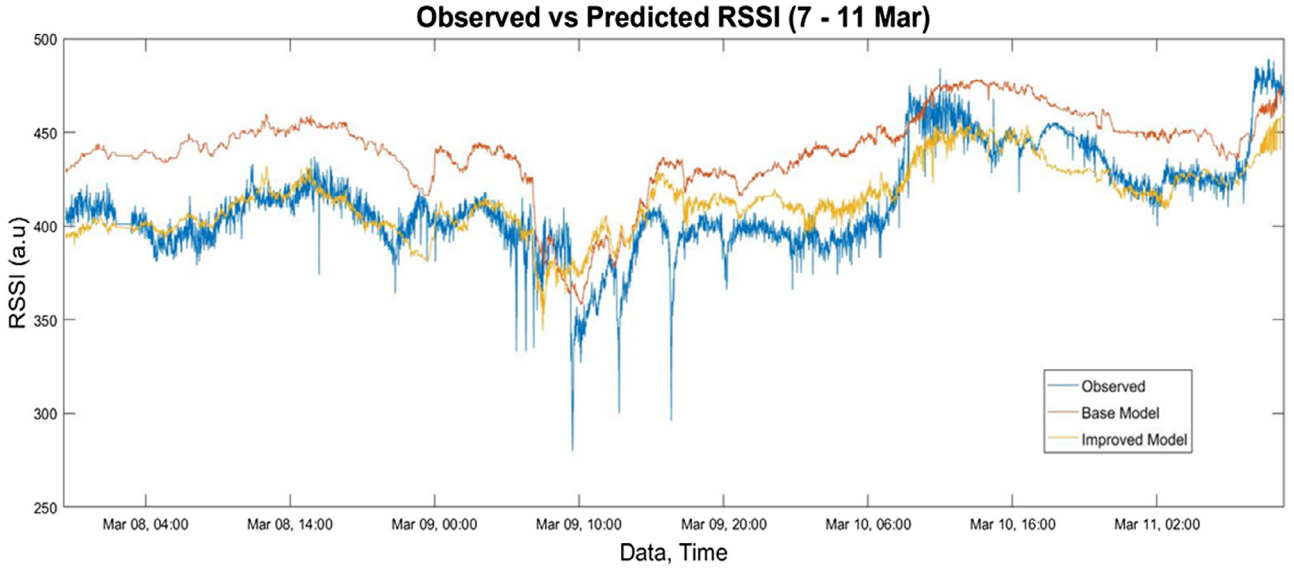


**Fig. 7.** Observed *RSSI* parameter as compared to both the base [31] and the improved model for the period from 7 to 11 March 2020.

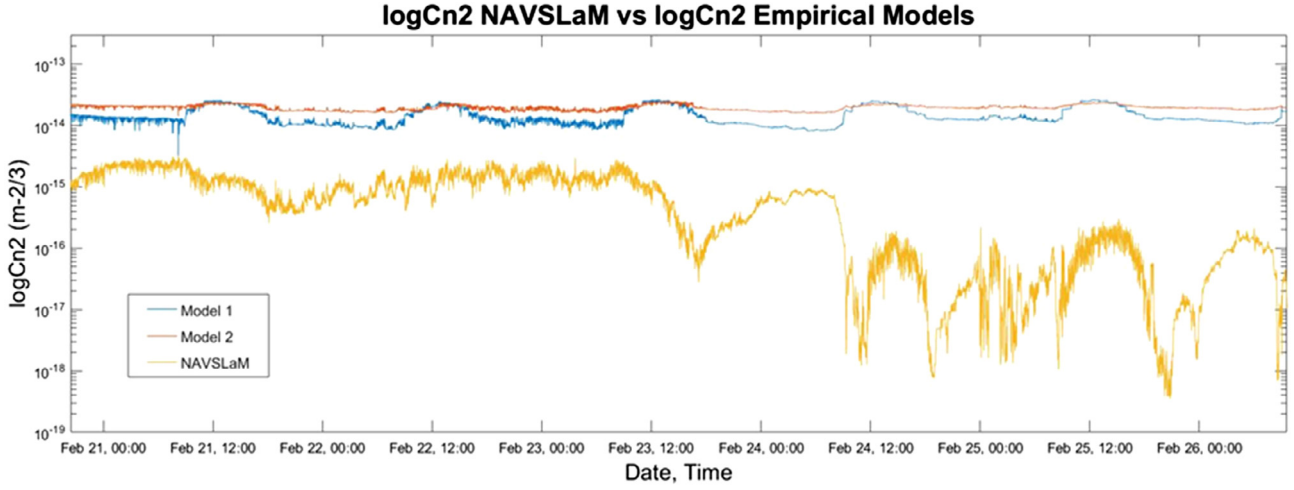


**Fig. 8.** Prediction of $C_n^2$ over the period from 20 to 26 Feb 20. NAVSLaM model (yellow line) as compared to empirical models [34, Eqs. 12,13].

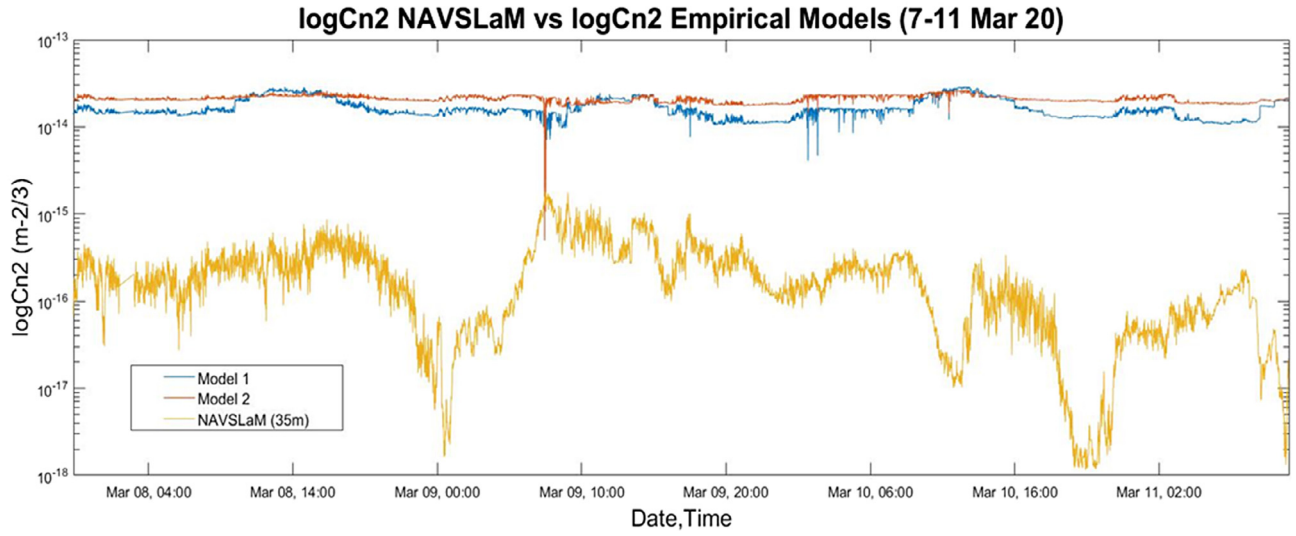


**Fig. 9.** Prediction of $C_n^{2.}$ over the period from 7 to 11 March 20. NAVSLaM model, i.e. yellow line, as compared to empirical models [34, Eqs. (12, 13)].

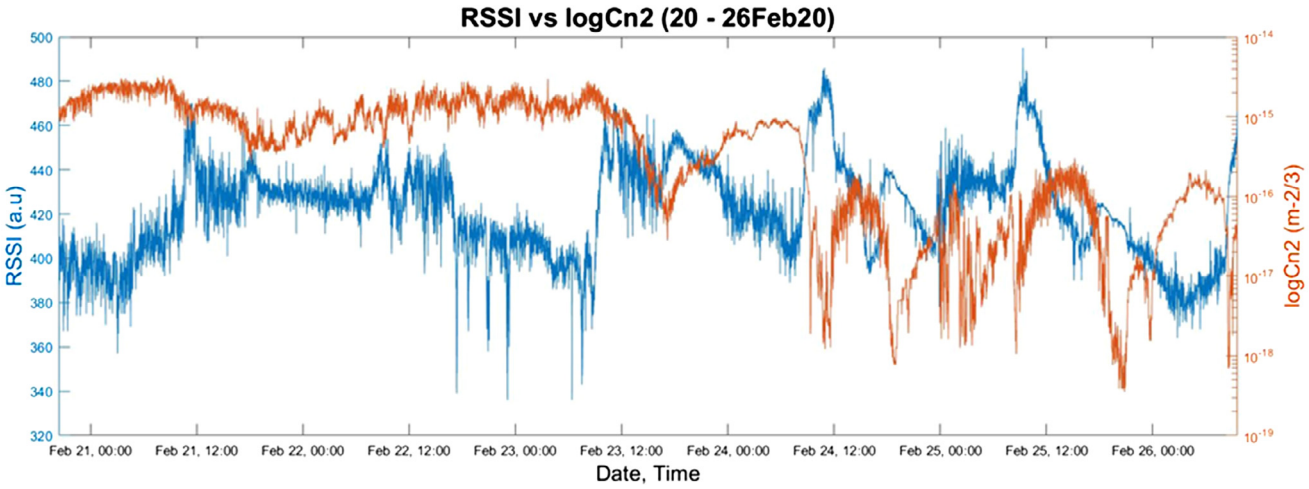


**Fig. 10.** *RSSI* versus $C_n^2$ for the period from 20 to 26 February 2020. A strong anti-correlated relation is observed. The $C_n^2$ is plotted in a logarithmic scale.

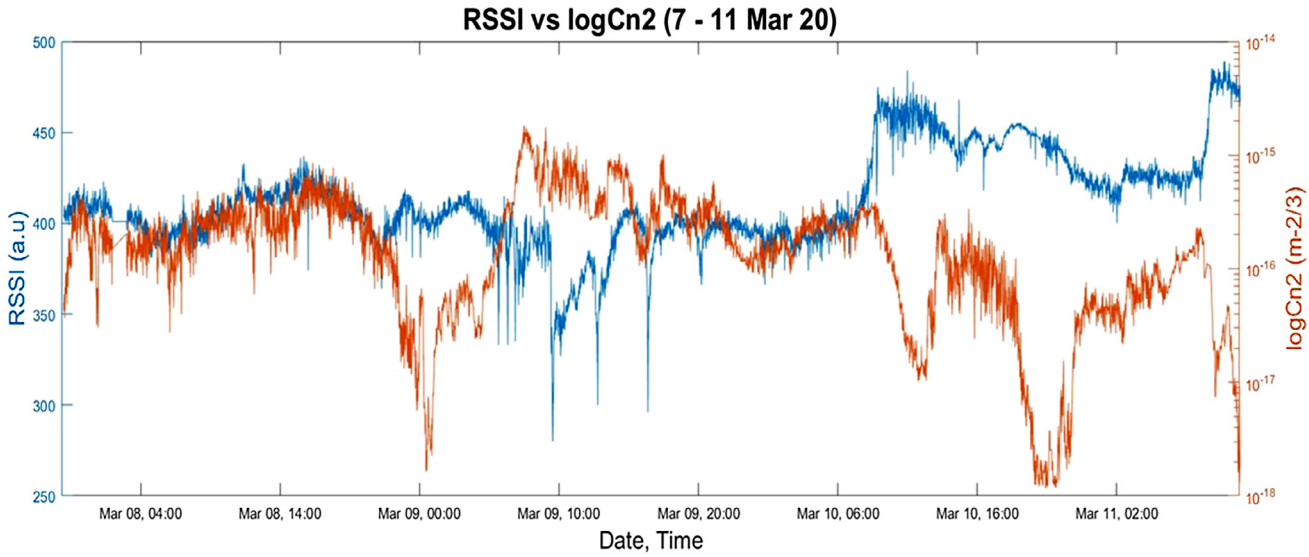


**Fig. 11.** *RSSI* versus $C_n^2$ for the period from 7 to 11 March 2020. Again a highly anti-correlated relation is observed. The $C_n^2$ value is plotted in a logarithmic scale.

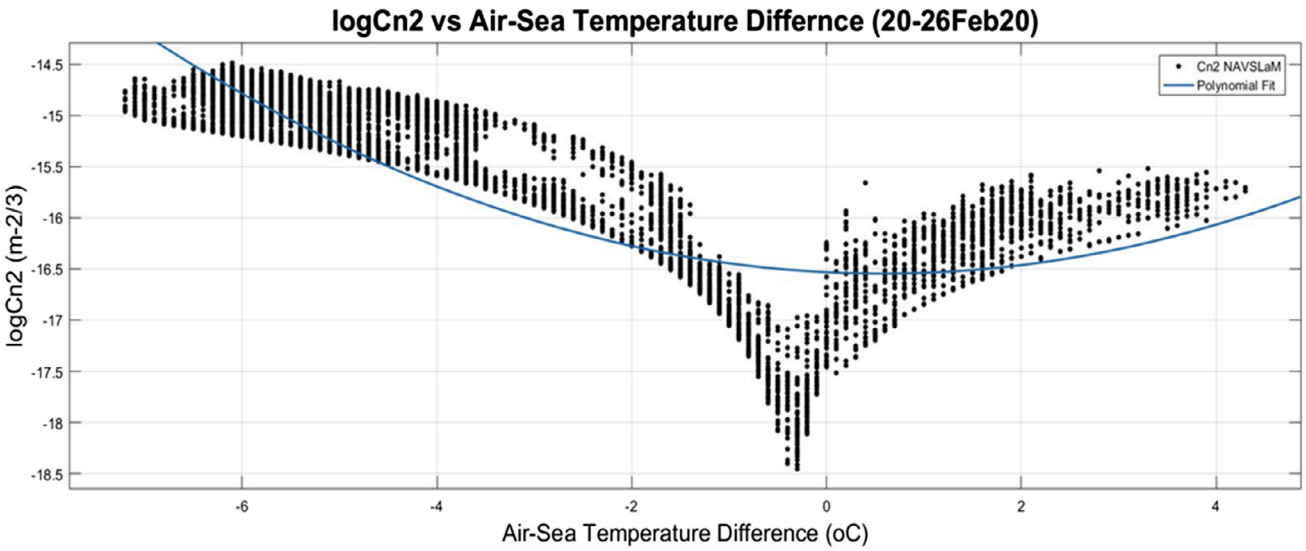


**Fig. 12.** $C_n^2$ measurements versus air–sea temperature difference for the period from 20 to 26 February 2020.

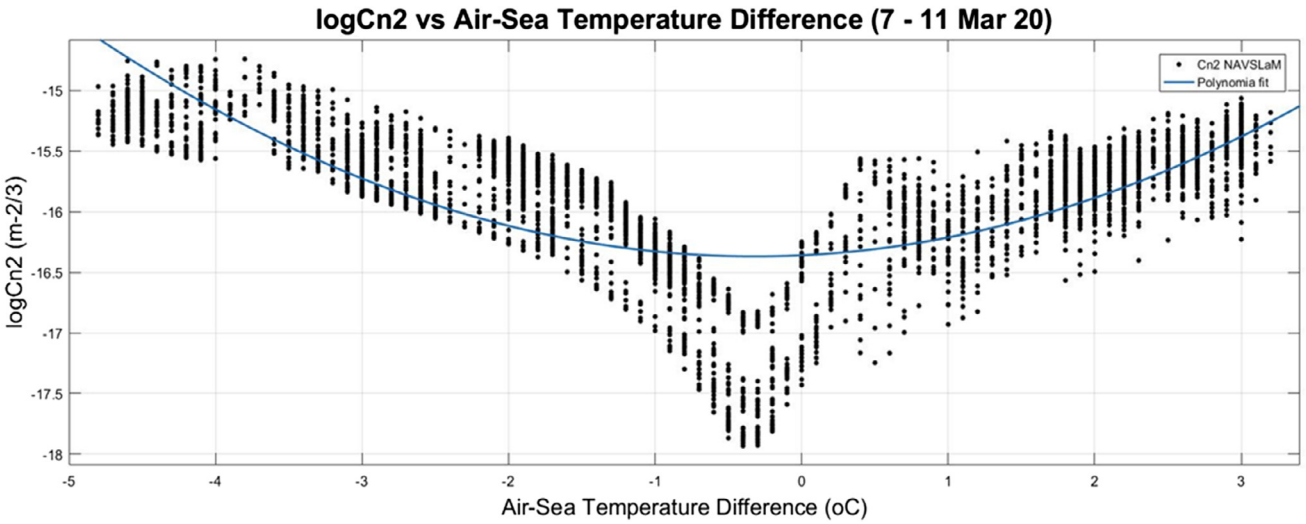


**Fig. 13.** $C_n^2$ measurements versus air–sea temperature difference for the period from 7 to 11 March 2020.

As previously stated the *ASTD* parameter value has a significant impact on the turbulence strength. During the two validation periods, both stable, i.e. *ASTD*> 0, and unstable, i.e. *ASTD*< 0; conditions occurred. During the first period, i.e. 20 to 26 February 2020, the *ASTD* had a mean value of −3.33 °C whereas during the second period the mean value was −0.57 °C. As shown in Figs. 12 and 13, as the ASTD parameter value approached to zero the atmospheric turbulence strength decreases, whereas for greater absolute values the turbulence increases.

The atmospheric turbulence is highly height-dependent. The highest values are observed at zero altitude, whereas significantly lower at higher altitudes [4]. For positive ASTD values the $C_n^2$ profile initially has larger gradient with height near zero height and then becomes less dependent on height than for negative *ASTD* values [37]. Fig. 14, shows the height dependence of $C_n^2$ for a typical midday and sunset time. It is obvious that the turbulence strength differs by an order of magnitude between the value at the surface and a height of 35 m, where our experimental setup is located. This fact would favor FSO systems in maritime platforms that are set in the highest possible location.

## 5. Conclusions

In this paper, we proposed a statistical model that significantly improves the accuracy of previous presented ones to predict the received signal strength of an FSO optical link over a maritime environment. A commercial FSO communication system and the appropriate weather station provided the required data. A closed form expression is constructed that predicts *RSSI* parameter based upon point measurements of local environmental parameters, such as wind speed, air temperature, humidity, pressure, dew point, solar flux and air–sea temperature difference. The latter has been found to have a significant impact on the laser beam propagation over sea. The regression analysis output showed a significant fit between measured and predicted *RSSI* values, that is certified by an $R^2$ parameter value of 71.1%. A linear correlation coefficient was also used to numerically evaluate their analogy, i.e. 0.843. We then validated our model and its ability to predict the *RSSI* parameter from macroscopic environmental point-measurements, during two distinct periods, the first from 20 to 26 February 2020 and the second from 7 to 11 March 2020. Overall, the improved model achieved a significant linear correlation coefficient of 0.78 with the observed values as compared to 0.73 of the base model for the first period

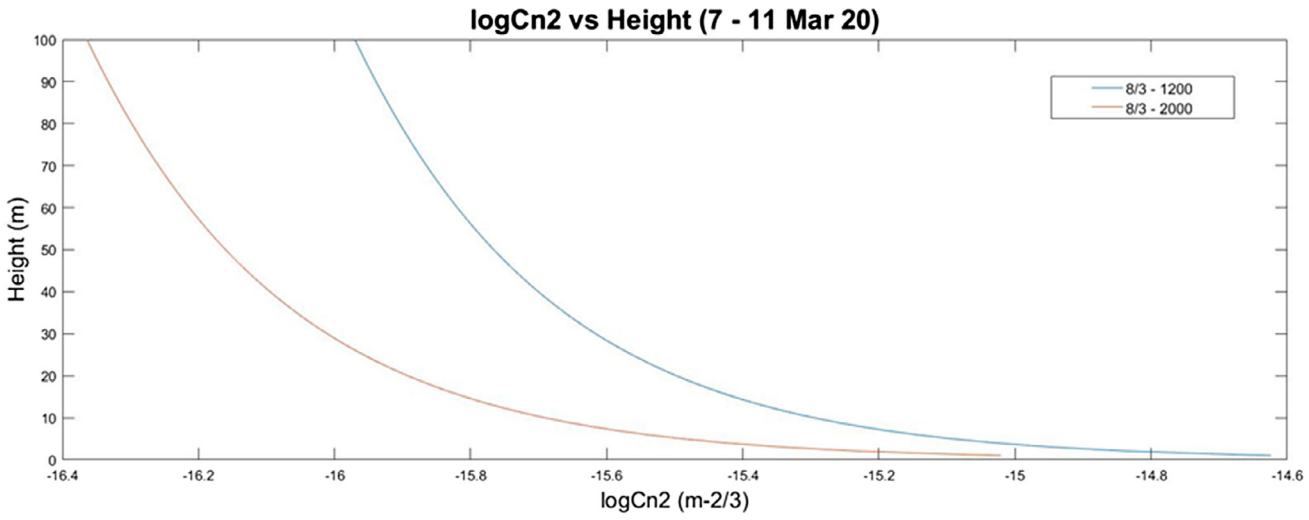


**Fig. 14.** Height dependence of $C_n^2$ for a typical midday (blue line) and sunset (red line) time.

and 0.81 as compared to 0.79 for the second period. The goodness of fit parameter $R^2$ between the improved model prediction and the observed values was 70.5% and 66% for the two periods, respectively. We then used the NAVSLaM model to estimate the $C_n^2$ during both validation periods and compared it to other empirical models that are not focused for a maritime environment; NAVSLaM predicted significantly lower $C_n^2$ values with a different diurnal profile from the classic bell-shaped one. The relation between the *RSSI* parameter and $C_n^2$ was also analyzed and proved to be highly anti-correlated for both validation periods. Finally, we investigated the relation between the *ASTD* and the $C_n^2$, which showed a clear trend towards lower $C_n^2$ values for *ASTD* around zero and higher $C_n^2$ values for higher absolute values of *ASTD*.

## Declaration of competing interest

The authors declare that they have no known competing financial interests or personal relationships that could have appeared to influence the work reported in this paper.

## References

[1] C.I. Moore, H.R. Burris, M.F. Stell, L. Wasiczko, M.R. Suite, R. Mahon, W.S. Rabinovich, G.C. Gilbreath, W.J. Scharpf, Atmospheric turbulence studies of a 16-km maritime path, in: Proceedings of the SPIE 5793, Atmospheric Propagation II, Orlando, FL, USA, 25 May 2005.

[2] K.J. Grant, K.A. Murry, B.A. Clare, A.S. Perejma, W.S. Martinsen, Maritime Laser Communications Trial, General Document, Defense Science and Technology Organization, Edimburg South Australia, June 2012.

[3] A. Malik, P. Singh, Free space optics: Current applications and future challenges, Int. J. Opt. 2015 (2015) 945483, http://dx.doi.org/10.1155/2015/945483.

[4] A. Lionis, K. Cohn, C. Pogue, Experimental design of a UCAV-based high energy laser weapon, Nausivios Chora J. 6 (2016) 3–17.

[5] H. Kaushal, G. Kaddoum, Underwater optical wireless communication, IEEE Access 4 (2016) 1518–1547.

[6] M. Jing, T. Liying, Y. Siyuan, Technologies and applications of free space optical communication and space optical information network, J. Commun. Inf. Netw. 1 (2016) 61–71.

[7] W.S. Rabinovich, C.I. Moore, R. Mahon, P.G. Goetz, H.R. Burris, M.S. Ferraro, J.L. Murphy, L.M. Thomas, G.C. Gilbreath, M. Vilcheck, M.R. Suite, Free-space optical communications research and demonstrations at the U.S. Naval Research Laboratory, Appl. Opt. 54 (2015) F189–F200.

[8] S. Doss-Hammel, D. Tsindikidis, D. Merritt, J. Fontana, Atmospheric characterization for high energy laser beam propagation in the maritime environment, in: Atmospheric Tracking, Imaging and Compensation, Proceedings of the SPIE 5552, Bellingham, WA, 2004; Michael T. Valley, Mikhail Vorontsov.

[9] A.N. De Jong, P.B. Schwering, A.M. Van Eijk, W.H. Gunter, Validation of atmospheric propagation models in littoral waters, Opt. Eng. 52 (4) (2013) 046002.

[10] Rita Mahon; Christopher I. Moore; Harris R. Burris; William S. Rabinovich; Michele R. Suite; Linda M. Thomas, Power spectra of a free space optical link in a maritime environment, in: Proc. SPIE 7464, Free-Space Laser Communications IX, 2009, 746407, http://dx.doi.org/10.1117/12.828860.

[11] E.S. Oh, J.C. Ricklin, G.C. Gilbreath, N.J. Vallestero, F.D. Eaton, Optical turbulence model for laser propagation and imaging applications, in: Proc. SPIE 5160, Free-Space Laser Communications and Active Laser Illumination III, Bellingham, WA, 2004, http://dx.doi.org/10.1117/12.504556.

[12] E.S. Oh, J.C. Ricklin, G.C. Gilbreath, S. Doss-Hammel, F.D. Eaton, C. Moore, J. Murphy, Y. Han Oh, M. Stell, Estimating optical turbulence using the PAMELA model, in: Proc. SPIE 5550, Free-Space Laser Communications IV, Bellingham, WA, 2004, http://dx.doi.org/10.1117/12.561481.

[13] F.S. Vetelino, C. Young, K. Grant, L. Wasiczko, H. Burris, C. Moore, R. Mahon, M. Suite, K. Corbett, B. Clare, C. Gilbreath, W. Rabinovich, Initial measurements of atmospheric parameters in a marine environment, in: Proc. SPIE 6215, Atmospheric Propagation III, Orlando, FL, 2006, http://dx.doi.org/10.1117/12.668026.

[14] L.M. Wasiczko, C.I. Moore, H.R. Burris, M. Suite, M. Stell, J. Murphy, G.C. Gilbreath, W. Rabinovich, W. Scharpf, Characterization of the Marine Atmosphere for Free-Space Optical Communication, in: Proceedings of the SPIE 6215, Atmospheric Propagation III, Orlando (Kissimmee), FL, USA, 17 May 2006.

[15] G.C. Gilbreath, W.S. Rabinovich, C.I. Moore, H.R. Burris, R. Mahon, K.J. Grant, P.G. Goetz, J.L. Murphy, M.R. Suite, M.F. Stell, M.L. Swingen, L.M. Wasiczko, S.R. Restaino, C. Wilcox, J.R. Andrews, W.J. Scharpf, Progress in laser propagation in a maritime environment at the naval research laboratory, in: Proc. SPIE 5892. Free-Space Laser Communications V, Bellingham, WA, 2005, http://dx.doi.org/10.1117/12.633390.

[16] H.R. Burris, C.I. Moore, L.A. Swingen, M.J. Vilcheck, D.A. Tulchinsky, R. Mahond, L.M. Wasiczko, M.F. Stell, M.R. Suite, M.A. Davis, S.W. Moore, W.S. Rabinovich, J.L. Murphy, G.C. Gilbreath, J. Scharpf, Latest results from the 32km maritime lasercom link at the naval research laboratory, chesapeake bay lasercom test facility, in: Proc. SPIE 5793. Atmospheric Propagation II, Bellingham, WA, 2005, http://dx.doi.org/10.1117/12.606030.

[17] C.I. Moore, H.R. Burris, W.S. Rabinovich, L. Wasiczko, M.R. Suite, L.A. Swingen, R. Mahon, M.F. Stell, G.C. Gilbreath, W.J. Scharpf, Overview of NRL's maritime laser communication test facility, in: Proc. SPIE 5892. Free-Space Laser Communications V, Bellingham, WA, 2005, http://dx.doi.org/10.1117/12.622252.

[18] S. Michael, R.R. Parenti, F.G. Walther, A.M. Volpicelli, J.D. Moores, W.W. Jr., R. Murphy, Comparison of Scintillation Measurements from a 5 km Communications Link to Standard Statistical Models, in: Proceedings of the SPIE 7324, Atmospheric Propagation VI, Orlando, FL, USA, 2 May 2009.

[19] John D. Moores, et al., Architecture overview and data summary ofa 5.4 km free-space laser communication experiment, in: Arun K. Majumdar, Christopher C. Davis (Eds.), Free-SpaceLaser Communications IX, SPIE, San Diego, CA, USA, 2009.

[20] J. Latal, J. Vitasek, L. Hajek, A. Vanderka, P. Koudelka, S. Kepak, V. Vasinek, Regression models utilization for RSSI prediction of professional FSO link with regards to atmosphere phenomena in proceedings of the 2016, in: International Conference on Broadband Communications for Next Generation Networks and Multimedia Applications (CoBCom), Graz, Austria, 14–16 September 2016.

[21] J. Latal, L. Hajek, A. Vanderka, J. Vitasek, P. Koudelka, S. Hejduk, Real measurements and evaluation of the influence of atmospheric phenomena on FSO combined with modulation formats, Electronics 20 (2016) http://dx.doi.org/10.7251/ELS1620062L.

[22] L. Hajek, J. Vitasek, A. Vanderka, J. Latal, F. Perecar, V. Vasinek, Statistical prediction of the atmospheric behavior for free space optical link, in: Proceedings of the SPIE 9614, Laser Communication and Propagation through the Atmosphere and Oceans IV, San Diego, CA, USA, 4 September 2015.

[23] W.G. Alheadary, K.-H. Park, N. Alfaraj, Y. Guo, E. Stegenburgs, T.K. Ng, B.S. Ooi, M.-S. Alouini, Free-space optical channel characterization and experimental validation in a coastal environment, Opt. Express 26 (2018) 6614–6628.

[24] W.G. Alheadary, K.-H. Park, B.S. Ooi, M.-S. Alouini, Free-space optical channel characterization in a coastal environment, J. Commun. Inf. Netw. 2 (2017) 100–106.

[25] A. Tunick, Statistical analysis of optical turbulence intensity over a 2.33 km propagation path, Opt. Expres 15 (2007) 3619–3628.

[26] A. Tunick, Optical turbulence parameters characterized via optical measurements over a 2.33-km free-space laser path, Opt. Express 16 (2008) 14645–14654.

[27] J. Yijun, M. Jing, T. Liying, Y. Siyuan, D. Wenhe, Measurement of optical intensity fluctuation over an 11.8 km turbulent path, Opt. Express 16 (2008) 6963–6973.

[28] A. Khandakar, A. Touati, F. Touati, A. Abdaoui, A. Bouallegue, Experimental setup to validate the effects of major environmental parameters on the performance of FSO communication link in Qatar, Appl. Sci. 8 (2018) 2599.

[29] D. Bourazani, A.N. Stasinakis, H.E. Nistazakis, G.K. Varotsos, A.D. Tsigopoulos, G.S. Tombras, Experimental accuracy investigation for irradiance fluctuations of FSO links modeled by gamma distribution, in: Proceedings of the 8th International Conference from Scientific Computing to Computational Engineering, Athens, Greece, 4–7 July 2018.

[30] M.N. Kampouraki, A.N. Stasinakis, H.E. Nistazakis, A.D. Tsigopoulos, G.S. Tombras, G.G. Chronopoulos, M.E. Fafalios, Experimental and theoretical bit rate estimation of turbulent FSO link over the maritime area at piraeus port, in: Proceedings of the 6th International Conference from Scientific Computing to Computational Engineering, Athens, Greece, 9–12 July, 2014.

[31] A. Lionis, K. Peppas, H.E. Nistazakis, A.D. Tsigopoulos, K. Cohn, Experimental performance analysis of an optical communication channel over maritime environment, Electronics 9 (2020) 1109.

[32] Hemani Kaushal, Vk Jain, Subrat Kar, Free-Space Optical Channel Models, 2017, http://dx.doi.org/10.1007/978-81-322-3691-7_2.

[33] R.J. Oermann, Novel Methods for the Quantification of Atmospheric Turbulence Strength in the Atmospheric Surface Layer (Ph.D. thesis), School of Chemistry and Physics, University of Adelaide, Adelaide SA, Australia, 2014.

[34] D. Sabot, N.S. Kopeika, Forecasting optical turbulence strength on the basis of macroscale meteorology and aerosols: models and validation, Opt. Eng. 31 (1992) http://dx.doi.org/10.1117/12.56059.

[35] R. Mahon, C. Moore, H. Burris, W. Rabinovich, M. Suite, L. Thomas, Power spectra of a free space optical link in a maritime environment, in: Proc. SPIE 7464, Free Space Laser Communications IX, San Diego, CA, 2009, http://dx.doi.org/10.1117/12.828860.

[36] S. Doss-Hammel, E. Oh, J. Ricklin, F. Eaton, C. Gilbreath, D. Tsindikidis, A comparison of optical turbulence models, in: Proc. SPIE 5550, Free Space Laser Communications IV, Bellingham, WA, 2004, http://dx.doi.org/10.1117/12.563746.

[37] P.A. Frederickson, K.L. Davidson, C.R. Zeisse, C.S. Bendall, Estimating the refractive index structure parameter ($Cn^2$) over the ocean using bulk methods, J. Appl. Meteorol. 39 (2000) 1770–1783.

[38] P. Frederickson, S. Hammel, D. Tsintikidis, Measurements and modeling of optical turbulence in a maritime environment, in: Proc SPIE, 2006, http://dx.doi.org/10.1117/12.683017.

[39] https://weather-stats.com/greece/athenes/sea_temperature#details.